AUT Journal of Mechanical Engineering

AUT J. Mech. Eng., 4(1) (2020) 103-118
DOI: 10.22060/ajme.2019.15375.5770

Time-Dependent Creep Response of Magneto-Electro-Elastic Rotating Disc in Thermal and Humid Environmental Condition

M. Saadatfar*

Department of Mechanical Engineering, University of Qom, Qom, Iran.

ABSTRACT: The aim of this paper is to analyze the time-dependent stress redistribution of a rotating magneto-electro-elastic disc. The disc is supposed to be placed in an axisymmetric temperature and moisture fields. Besides, the disc is under a centrifugal body force, an induced electric potential in addition to magnetic potential. Using equilibrium, electrostatic and magnetostatic equations, strain-displacement and stress-strain relations together with hygrothermal equations, a differential equation is obtained in which there are creep strains. Primarily, disregarding the creep strain, an analytical solution for the initial stresses, electromagnetic potentials and displacement is developed. Then, using Prandtl-Reuss relations, creep stress rates and electromagnetic potentials rates are obtained. Finally, the history of stresses, electric and magnetic potentials is obtained iteratively. In the numerical section, the influence of creep evolution, hygrothermal environmental condition, angular velocity and temperature- and moisture-dependency of elastic coefficients on the behavior of magneto-electro-elastic disc is analyzed comprehensively. The results show that the effect of hygrothermal loading and angular velocity becomes less significant after creep evolution. Also, the results imply that analysis of the effect of temperature- and moisture- dependence after creep evolution must be considered in the design progress. Besides, to avoid cracking, increasing in the tensile hoop stress at the internal surface with increasing in hygrothermal loading must be considered in design progress..

Review History:

Received: 1 Dec. 2018
Revised: 5 Feb. 2019
Accepted: 14 Apr. 2019
Available Online: 27 Apr. 2019

Keywords:

Rotating disc
Magneto-electro-elastic
Time-dependent creep
Hygrothermal loading

1. Introduction

Due to huge application of rotating disc in rotating machinery, they have been focused by many researchers. They have many industrial usages such as compressors, turbo generators, flywheels, gas turbine rotors, automotive braking systems, ship propellers and computer disc drives [1]. On the other hand, Magneto-Electro-Elastic (MEE) composites that are a type of intelligent materials have been focused by many researchers. Due to the presence of magnetic and electric coupling effect, these materials allow an extra degree of freedom in the design of actuators, sensors, storage devices and transducers. Their requests can be found in turbine rotors, aerospace, magnetic storage elements and magnetic structural elements.

Since smart materials are mostly selected to work in presence of magnetic field or in high temperature and humid environments [2], several papers are presented in the literature for static hygrothermal analysis of them. Akbarzadeh and Chen [3] presented a solution for hygrothermal stress problem in Functionally Graded Piezoelectric Material (FGPM) cylinder and spheres. Analysis of the interaction of electric field, elastic deformation, thermal and moisture condition in hollow and solid piezoelectric cylinders was presented by Allam et al [4]. Saadatfar and Aghaie-Khafri [5] analyzed the static response of a Functionally Graded MEE (FGMEE) thick-walled sphere in thermal and humid condition using an analytical method. A long Functionally Graded Material (FGM) cylindrical shell with FGPM sensor and actuators under magneto-thermo-electro-elastic loading was analyzed analytically by Saadatfar and Aghaie-Khafri [6]. Also, they illustrated that the actuation and sensing authority of FGPM layers mostly affected by the grading-index of the FGPM [7]. Then, they considered a FGM cylindrical shell integrated with FGPM layers subjected to magneto-thermo-electro-elastic [89] hygro-thermo-electro-elastic [10] and hygro-thermo-magneto-electro-elastic [11] loadings. A closed-form solution for a piezoelectric functionally graded fiber-reinforced hollow cylinder in hygrothermal condition was derived by Zenkour [12]. The static analysis of MEE plate in hygrothermal environment was presented by Vinyas and Kattimani [13] using the finite element method. Thermoelastic behavior of a rotating disc with variable thickness made of FGMEE was presented by Dai and Dai [14]. Also, several authors have tried to analyze the creep response of composite, FGM and smart discs. Using Sherby's law, the creep progress of an isotropic FGM rotating disk with thermal gradient was considered by Gupta et al. [15]. Creep behavior of FGM rotating disks with linearly varying thickness was investigated by Deepak et al. [16]. Rattan et al. [17] tried to

*Corresponding author's email: m.saadatfar@qom.ac.ir

analyze the creep progress of an isotropic rotating disk made of particle reinforced FGM. Dharmpal et al. [18] analyzed the steady-state stress redistribution in a FGM rotating disk with variable thickness. Gupta and Singh [19] made an attempt to present an analytical method to analyze the creep progress in non-FGM/FGM rotating disk with uniform and non-uniform thickness. The steady-state creep behavior of an isotropic rotating disk made of parabolically varying FGM in thermal environment is investigated by Bose and Rattan [20]. Loghman et al. [21] considered the creep response of FGPM rotating disc under magneto-electro-thermal loads using a semi-analytical method. They show that the history of electric potential can be used for condition monitoring of the smart disk without any need to destructive or non-destructive testing. A new analytical-numerical way to analyze creep evolution of rotating disk made of nonlinear piezoelectric polymer in thermal environmental condition was presented by Loghman and Azami [22]. They show that a significant electric potential redistribution due to stress redistribution has occurred during the lifetime of the disk.

Literature review reveals that creep analysis is vital for rotating disk. Also, smart materials are subjected to hygrothermal loading in some of their application. Moreover, they show considerable creep effects under severe environmental condition [23]. Therefore, to have advanced performance and reliability of intelligent structures, creep response must be investigated when MEE structures are used in hygrothermal environmental condition. However, the creep analysis has not been investigated for the MEE disc so far. So, the novelty of the present research is to investigate the time-dependent creep stress and electric and magnetic potentials redistributions during the lifetime of a MEE disc in steady-state hygrothermal environment considering-temperature and moisture- dependency of elastic constants using analytical methods.

2. Basic Formulation of the Problem

Consider a uniform thickness MEE disc rotates about z axis with a constant speed as shown in Fig. 1. The disc is assumed to be subjected to hygrothermal field in addition to electro-magnetic potentials at inner and outer surfaces. Regarding symmetry and plane stress condition, nonzero components of temperature, moisture concentration, electric potential, magnetic potential and displacement are function of radius.

2.1 Formulation of the hygrothermal field

In an uncoupled hygrothermal analysis, the temperature distribution as well as moisture concentration distribution can be achieved independently [24]. The Fourier heat conduction equation and Fickian moisture diffusion equation without source of heat and moisture for a disc in axisymmetric steady-state condition are expressed as [25,26]:

$$\frac{1}{r}\frac{\partial}{\partial r}(rk^{T}\frac{\partial T}{\partial r})=0, \tag{1-a}$$

$$\frac{1}{r}\frac{\partial}{\partial r}(rk^{C}\frac{\partial M}{\partial r})=0, \tag{1-b}$$

Integrating Eq. (1) twice gives:

$$\begin{aligned} T(r)&=W_1\ln(r)-W_2,\\ M(r)&=S_1\ln(r)-S_2. \end{aligned} \tag{2}$$

In this research, moisture concentration change M_a and M_b and temperatures change T_a and T_b are assumed at the inside and outside of the disc, respectively. The unknown constants can be achieved using these hygrothermal boundary conditions as:

$$\begin{aligned} W_1&=\frac{T_b-T_a}{\ln(\frac{b}{a})},\\ W_2&=\frac{T_b-T_a}{\ln(\frac{b}{a})}\ln(b)-T_b. \end{aligned} \tag{3-a}$$

$$\begin{aligned} S_1&=\frac{M_b-M_a}{\ln(\frac{b}{a})},\\ S_2&=\frac{M_b-M_a}{\ln(\frac{b}{a})}\ln(b)-M_b. \end{aligned} \tag{3-b}$$

2.2 Basic equations of the MEE rotating disc

The entire strains are supposed to be sum of magnetic, electric, elastic, hygrothermal, and creep strains. Therefore, the stress-strain relations can be written in the following form [25,27]:

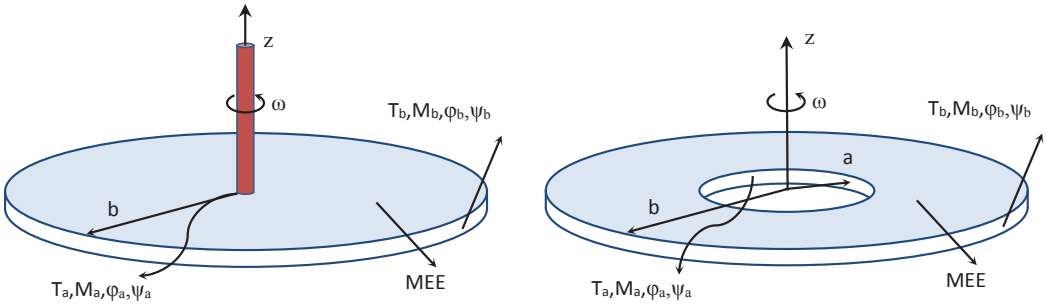

Fig. 1. MEE rotating disc

$$\sigma_r = c_{11}\left(\varepsilon_{rr}-\varepsilon_{rr}^c\right)+c_{12}\left(\varepsilon_{\theta\theta}-\varepsilon_{\theta\theta}^c\right)+ c_{13}\left(\varepsilon_{zz}-\varepsilon_{zz}^c\right)-e_{11}E_r-q_{11}H_r-\lambda_1 T-\zeta_1 M \tag{4-a}$$

$$\sigma_\theta = c_{12}\left(\varepsilon_{rr}-\varepsilon_{rr}^c\right)+c_{22}\left(\varepsilon_{\theta\theta}-\varepsilon_{\theta\theta}^c\right)+ c_{23}\left(\varepsilon_{zz}-\varepsilon_{zz}^c\right)-e_{12}E_r-q_{12}H_r-\lambda_2 T-\zeta_2 M \tag{4-b}$$

$$\sigma_z = c_{13}\left(\varepsilon_{rr}-\varepsilon_{rr}^c\right)+c_{23}\left(\varepsilon_{\theta\theta}-\varepsilon_{\theta\theta}^c\right)+ c_{33}\left(\varepsilon_{zz}-\varepsilon_{zz}^c\right)-e_{13}E_r-q_{13}H_r-\lambda_3 T-\zeta_3 M \tag{4-c}$$

$$D_r = e_{11}\left(\varepsilon_{rr}-\varepsilon_{rr}^c\right)+e_{12}\left(\varepsilon_{\theta\theta}-\varepsilon_{\theta\theta}^c\right)+ e_{13}\left(\varepsilon_{zz}-\varepsilon_{zz}^c\right)+\beta_{11}E_r+\varepsilon_{11}H_r+p_1 T+\chi_1 M, \tag{4-d}$$

$$B_r = q_{11}\left(\varepsilon_{rr}-\varepsilon_{rr}^c\right)+q_{12}\left(\varepsilon_{\theta\theta}-\varepsilon_{\theta\theta}^c\right)+ q_{13}\left(\varepsilon_{zz}-\varepsilon_{zz}^c\right)+\varepsilon_{11}E_r+d_{11}H_r+m_1 T+\gamma_1 M \tag{4-e}$$

where

$$\begin{aligned}\lambda_1 &= c_{11}\alpha_r + c_{12}\alpha_\theta + c_{13}\alpha_z\\ \lambda_2 &= c_{12}\alpha_r + c_{22}\alpha_\theta + c_{23}\alpha_z\\ \lambda_3 &= c_{13}\alpha_r + c_{23}\alpha_\theta + c_{33}\alpha_z\end{aligned} \tag{5-a}$$

$$\begin{aligned}\zeta_1 &= c_{11}\beta_r + c_{12}\beta_\theta + c_{13}\beta_z\\ \zeta_2 &= c_{12}\beta_r + c_{22}\beta_\theta + c_{23}\beta_z\\ \zeta_3 &= c_{13}\beta_r + c_{23}\beta_\theta + c_{33}\beta_z\end{aligned} \tag{5-b}$$

The equilibrium equation of the rotating MEE disc is presented as [14,21]:

$$\frac{\partial \sigma_r}{\partial r}+\frac{(\sigma_r-\sigma_\theta)}{r}+\rho r\omega^2 = 0. \tag{6}$$

Without electric charge and electric current densities, the electrostatic and magnetostatic equations can be written as [14,25]:

$$\frac{\partial D_r}{\partial r}+\frac{D_r}{r}=0, \tag{7-a}$$

$$\frac{\partial B_r}{\partial r}+\frac{B_r}{r}=0. \tag{7-b}$$

Two types of mechanical boundary condition are taken named Fixed-Free and Free-Free boundary conditions [22,28]. Also, the inner and outer surface is subjected to electric potential and magnetic potential. These boundary conditions can be presented as:

$$\begin{aligned}&\text{Fixed}-\text{Free}\rightarrow u_r\big|_{r=a}=0, \qquad \sigma_r\big|_{r=b}=0,\\ &\text{Free}-\text{Free}\rightarrow \sigma_r\big|_{r=a}=0, \qquad \sigma_r\big|_{r=b}=0,\\ &\phi\big|_{r=a}=\phi_a, \qquad \phi\big|_{r=b}=\phi_b,\\ &\psi\big|_{r=a}=\psi_a, \qquad \psi\big|_{r=b}=\psi_b.\end{aligned} \tag{8}$$

Solving Eq. (7), gives:

$$D_r = \frac{A_1}{r}, \tag{9-a}$$

$$B_r = \frac{A_2}{r}, \tag{9-b}$$

where, A_1 and A_2 are unknown constants. Due to plane stress condition, the z component of stress is set to zero. So, we have:

$$\sigma_z = 0 \Rightarrow \left(\varepsilon_{zz}-\varepsilon_{zz}^c\right) = -\frac{c_{13}}{c_{33}}\left(\varepsilon_{rr}-\varepsilon_{rr}^c\right)- \frac{c_{23}}{c_{33}}\left(\varepsilon_{\theta\theta}-\varepsilon_{\theta\theta}^c\right)+\frac{e_{13}}{c_{33}}E_r+\frac{q_{13}}{c_{33}}H_r+\frac{\lambda_3}{c_{33}}T+\frac{\zeta_3}{c_{33}}M \tag{10}$$

Also, we know that:

$$\varepsilon_{rr}=\frac{\partial u}{\partial r}, \quad \varepsilon_{\theta\theta}=\frac{u}{r}, \qquad E_r=-\frac{\partial \phi}{\partial r}, \quad H_r=-\frac{\partial \psi}{\partial r} \tag{11}$$

Using Eqs. (10) and (11), the Eq. (4) can be rewritten as:

$$\sigma_r = c'_{11}\frac{\partial u}{\partial r}+c'_{12}\frac{u}{r}+e'_{11}\frac{\partial \phi}{\partial r}+ q'_{11}\frac{\partial \psi}{\partial r}-\lambda'_1 T-\zeta'_1 M-c'_{11}\varepsilon_{rr}^c-c'_{12}\varepsilon_{\theta\theta}^c \tag{12-a}$$

$$\sigma_\theta = c'_{12}\frac{\partial u}{\partial r}+c'_{22}\frac{u}{r}+e'_{12}\frac{\partial \phi}{\partial r}+q'_{12}\frac{\partial \psi}{\partial r}- \lambda'_2 T-\zeta'_2 M-c'_{12}\varepsilon_{rr}^c-c'_{22}\varepsilon_{\theta\theta}^c \tag{12-b}$$

$$D_r = e'_{11}\frac{\partial u}{\partial r}+e'_{12}\frac{u}{r}-\beta'_{11}\frac{\partial \phi}{\partial r}-\varepsilon'_{11}\frac{\partial \psi}{\partial r}+ p'_1 T+\chi'_1 M-e'_{11}\varepsilon_{rr}^c-e'_{12}\varepsilon_{\theta\theta}^c, \tag{12-c}$$

$$B_r = q'_{11}\frac{\partial u}{\partial r}+q'_{12}\frac{u}{r}-\varepsilon'_{11}\frac{\partial \phi}{\partial r}-d'_{11}\frac{\partial \psi}{\partial r}+ m'_1 T+\gamma'_1 M-q'_{11}\varepsilon_{rr}^c-q'_{12}\varepsilon_{\theta\theta}^c \tag{12-d}$$

where

$$c'_{11}=c_{11}-\frac{c_{13}^2}{c_{33}}, \qquad c'_{12}=c_{12}-\frac{c_{13}c_{23}}{c_{33}},$$

$$c'_{22}=c_{22}-\frac{c_{23}^2}{c_{33}},\qquad \chi'_1=\chi_1+\frac{e_{13}\zeta_3}{c_{33}}$$
$$e'_{11}=e_{11}-\frac{c_{13}e_{13}}{c_{33}},\quad e'_{12}=e_{12}-\frac{c_{23}e_{13}}{c_{33}},$$
$$q'_{11}=q_{11}-\frac{c_{13}q_{13}}{c_{33}},\quad q'_{12}=q_{12}-\frac{c_{23}q_{13}}{c_{33}},$$
$$\lambda'_1=\lambda_1-\frac{c_{13}\lambda_3}{c_{33}},\quad \lambda'_2=\lambda_2-\frac{c_{23}\lambda_3}{c_{33}},$$
$$\zeta'_1=\zeta_1-\frac{c_{13}\zeta_3}{c_{33}},\qquad \zeta'_2=\zeta_2-\frac{c_{23}\zeta_3}{c_{33}} \tag{13}$$
$$\gamma'_1=\gamma_1+\frac{\zeta_3 q_{13}}{c_{33}},\qquad m'_1=m_1+\frac{\lambda_3 q_{13}}{c_{33}},$$
$$d'_{11}=d_{11}+\frac{q_{13}^2}{c_{33}},\qquad \beta'_{11}=\beta_{11}+\frac{e_{13}^2}{c_{33}},$$
$$\varepsilon'_{11}=\varepsilon_{11}+\frac{e_{13}q_{13}}{c_{33}},\quad p'_1=p_1+\frac{e_{13}\lambda_3}{c_{33}},$$

Substituting Eq. (9) into Eqs. (12-c) and (12-d), after rearranging, gives:

$$\frac{\partial\phi(r)}{\partial r}=\begin{pmatrix} L_1\dfrac{\partial u}{\partial r}+L_2\dfrac{u}{r}+L_3\dfrac{A_2}{r}+L_4T+\\ L_6M-L_5\dfrac{A_1}{r}-L_1\varepsilon^c_{rr}-L_2\varepsilon^c_{\theta\theta}\end{pmatrix} \tag{14-a}$$

$$\frac{\partial\psi(r)}{\partial r}=\begin{pmatrix} P_1\dfrac{\partial u}{\partial r}+P_2\dfrac{u}{r}+P_3\dfrac{A_1}{r}+P_4T+\\ P_6M-P_5\dfrac{A_2}{r}-P_1\varepsilon^c_{rr}-P_2\varepsilon^c_{\theta\theta}\end{pmatrix} \tag{14-b}$$

where:

$$L_1=\frac{e'_{11}d'_{11}-\varepsilon'_{11}q'_{11}}{\beta'_{11}d'_{11}-\varepsilon'^2_{11}},\quad L_2=\frac{e'_{12}d'_{11}-\varepsilon'_{11}q'_{12}}{\beta'_{11}d'_{11}-\varepsilon'^2_{11}},$$
$$L_3=\frac{\varepsilon'_{11}}{\beta'_{11}d'_{11}-\varepsilon'^2_{11}},\quad L_4=\frac{d'_{11}p'_1-\varepsilon'_{11}m'_1}{\beta'_{11}d'_{11}-\varepsilon'^2_{11}},$$
$$L_5=\frac{d'_{11}}{\beta'_{11}d'_{11}-\varepsilon'^2_{11}},\quad L_6=\frac{d'_{11}\chi'_1-\varepsilon'_{11}\gamma'_1}{\beta'_{11}d'_{11}-\varepsilon'^2_{11}},$$
$$P_1=\frac{q'_{11}\beta'_{11}-\varepsilon'_{11}e'_{11}}{\beta'_{11}d'_{11}-\varepsilon'^2_{11}},\quad P_2=\frac{q'_{12}\beta'_{11}-e'_{12}\varepsilon'_{11}}{\beta'_{11}d'_{11}-\varepsilon'^2_{11}}, \tag{15}$$
$$P_3=\frac{\varepsilon'_{11}}{\beta'_{11}d'_{11}-\varepsilon'^2_{11}},\quad P_4=\frac{\beta'_{11}m'_1-\varepsilon'_{11}p'_1}{\beta'_{11}d'_{11}-\varepsilon'^2_{11}},$$
$$P_5=\frac{\beta'_{11}}{\beta'_{11}d'_{11}-\varepsilon'^2_{11}},\quad P_6=\frac{\beta'_{11}\gamma'_1-\varepsilon'_{11}\chi'_1}{\beta'_{11}d'_{11}-\varepsilon'^2_{11}},$$

Substituting Eq. (14) into Eqs. (12-a) and (12-b) gives:

$$\sigma_r=C_1\frac{\partial u}{\partial r}+C_2\frac{u}{r}+C_3\frac{A_2}{r}+C_4\frac{A_1}{r}+C_5T+ C_6M-\lambda'_1T-\zeta'_1M-C_1\varepsilon^c_{rr}-C_2\varepsilon^c_{\theta\theta}, \tag{16-a}$$

$$\sigma_\theta=E_1\frac{\partial u}{\partial r}+E_2\frac{u}{r}+E_3\frac{A_2}{r}+E_4\frac{A_1}{r}+E_5T+ E_6M-\lambda'_2T-\zeta'_2M-E_1\varepsilon^c_{rr}-E_1\varepsilon^c_{\theta\theta}, \tag{16-b}$$

where,

$$C_1=c'_{11}+e'_{11}L_1+q'_{11}P_1,\qquad C_2=c'_{12}+e'_{11}L_2+q'_{11}P_2,$$
$$C_3=e'_{11}L_3-q'_{11}P_5,\qquad C_4=-e'_{11}L_5+q'_{11}P_3,$$
$$C_5=e'_{11}L_4+q'_{11}P_4,\qquad C_6=e'_{11}L_6+q'_{11}P_6, \tag{17}$$
$$E_1=c'_{12}+e'_{12}L_1+q'_{12}P_1,\qquad E_2=c'_{22}+e'_{12}L_2+q'_{12}P_2,$$
$$E_3=e'_{12}L_3-q'_{12}P_5,\qquad E_4=-e'_{12}L_5+q'_{12}P_3,$$
$$E_5=e'_{12}L_4+q'_{12}P_4,\qquad E_6=e'_{12}L_6+q'_{12}P_6$$

Substituting Eq. (16) into Eq. (6), the equilibrium equation is now can be expressed as:

$$\frac{\partial^2u}{\partial r^2}+\frac{1}{r}M_1\frac{\partial u}{\partial r}+\frac{1}{r^2}M_2u=+M_3r^{-1}T+M_4\frac{T}{r}+ \left(-M_5+M_6\right)\frac{\partial T}{\partial r}+M_7\frac{A_2}{r^2}+M_8\frac{A_1}{r^2}+M_9r^{-1}M+ M_{10}\frac{M}{r}+\left(-M_{11}+M_{12}\right)\frac{\partial M}{\partial r}-M_{13}r+ M_{14}r^{-1}\varepsilon^c_{rr}+\frac{\partial\varepsilon^c_{rr}}{\partial r}+M_{15}r^{-1}\varepsilon^c_{\theta\theta}+M_{16}\frac{\partial\varepsilon^c_{\theta\theta}}{\partial r} \tag{18}$$

where,

$$M_1=\frac{C_1+C_2-E_1}{C_1},\quad M_2=\frac{-E_2}{C_1},$$
$$M_3=\frac{\left(\lambda_1-\lambda_2\right)}{C_1},\qquad M_4=\frac{E_5-C_5}{C_1},$$
$$M_5=\frac{C_5}{C_1},\quad M_6=\frac{\lambda_1}{C_1},\quad M_7=\frac{E_3}{C_1},$$
$$M_8=\frac{E_4}{C_1},\quad M_9=\frac{\left(\zeta_1-\zeta_2\right)}{C_1}, \tag{19}$$
$$M_{10}=\frac{E_6-C_6}{C_1},M_{11}=\frac{C_6}{C_1},\quad M_{12}=\frac{\zeta_1}{C_1},$$
$$M_{13}=\frac{\rho\omega^2}{C_1},\quad M_{14}=\frac{2C_1-2E_1}{C_1},$$
$$M_{15}=\frac{2C_2-2E_2}{C_1},\quad M_{16}=\frac{C_2}{C_1}$$

3. Solution of the Equations

3.1 Primitive hygrothermal analysis of the MEE rotating disc

To find initial stresses, eliminating creep strains in the differential equation of Eq. (28), we have:

$$\frac{\partial^2 u}{\partial r^2}+\frac{M_1}{r}\frac{\partial u}{\partial r}+\frac{M_2}{r^2}u=\begin{pmatrix}-M_3W_2-M_9S_2-\\ M_4W_2-M_{10}S_2-\\ M_5W_1+M_6W_1-\\ M_{11}S_1+M_{12}S_2\end{pmatrix}r^{-1}+\left(W_1M_3+S_1M_9+W_1M_4+S_1M_{10}\right)\ln(r)r^{-1}+M_7A_2r^{-2}+M_8A_1r^{-2}-M_{13}r \tag{20}$$

The complete solution of Eq. (20) may be considered as: where B1 and B2 are unknown constants and:

$$u=B_1r^{m_1}+B_2r^{m_2}+B_3r+B_6r^3+B_7A_2+B_8A_1-\frac{B_5r}{(1-m_1)(m_2-m_1)}\left(\ln(r)-\frac{1}{1-m_1}\right)+\frac{B_5r}{(1-m_2)(m_2-m_1)}\left(\ln(r)-\frac{1}{1-m_2}\right) \tag{21}$$

Using Eq. (21) in Eq. (14-a) and then integrating, one has:

$$m_{1,2}=\frac{1}{2}\left(-(M_1-1)\pm\sqrt{(M_1-1)^2-4M_2}\right),\quad B_8=\frac{M_8}{M_2},\quad B_7=\frac{M_7}{M_2},$$
$$B_3=\frac{-M_4W_2-M_{10}S_2-M_3W_2-M_9S_2-M_{11}S_1+M_{12}S_2-M_5W_1+M_6W}{M_1+M_2},$$
$$B_5=\frac{W_1M_4+S_1M_{10}+W_1M_3+S_1M_9}{M_1+M_2},\quad B_6=\frac{-M_{13}}{6+3M_1+M_2}, \tag{22}$$

where, Z1 is an unknown constant. With a similar method, is

$$\phi(r)=L_1\left(B_1r^{m_1}+B_2r^{m_2}+B_3r+B_5+B_6r^3-\frac{B_5}{(1-m_1)(m_2-m_1)}\left(r\ln(r)-2r-\frac{r}{1-m_1}\right)-\frac{B_5}{(1-m_2)(m_2-m_1)}\left(r\ln(r)-2r-\frac{r}{1-m_2}\right)\right)+L_2\left(\frac{B_1}{m_1}r^{m_1}+\frac{B_2}{m_2}r^{m_2}+B_3r+\frac{B_6}{3}r^3+\left(B_7A_2+B_8A_1\right)\ln(r)-\frac{B_5r}{(1-m_1)(m_2-m_1)}\left(\ln(r)-1-\frac{1}{1-m_1}\right)+\frac{B_5r}{(1-m_2)(m_2-m_1)}\left(\ln(r)-1-\frac{1}{1-m_2}\right)\right)+L_4\left(W_1r\ln(r)-W_1r+W_2r\right)+L_6\left(S_1r\ln(r)-S_1r+S_2r\right)+\left(-L_5A_1+L_3A_2\right)\ln(r)+Z_1 \tag{23}$$

achieved as:

$$\psi(r)=P_1\left(B_1r^{m_1}+B_2r^{m_2}+B_3r+B_5+B_6r^3-\frac{B_5}{(1-m_1)(m_2-m_1)}\left(r\ln(r)-2r-\frac{r}{1-m_1}\right)-\frac{B_5}{(1-m_2)(m_2-m_1)}\left(r\ln(r)-2r-\frac{r}{1-m_2}\right)\right)+P_2\left(\frac{B_1}{m_1}r^{m_1}+\frac{B_2}{m_2}r^{m_2}+B_3r+\frac{B_6}{3}r^3+\left(B_7A_2+B_8A_1\right)\ln(r)-\frac{B_5r}{(1-m_1)(m_2-m_1)}\left(\ln(r)-1-\frac{1}{1-m_1}\right)+\frac{B_5r}{(1-m_2)(m_2-m_1)}\left(\ln(r)-1-\frac{1}{1-m_2}\right)\right)+P_4\left(W_1r\ln(r)-W_1r+W_2r\right)+P_6\left(S_1r\ln(r)-S_1r+S_2r\right)+\left(-P_5A_1+P_3A_2\right)\ln(r)+Z_2 \tag{24}$$

where, Z_2 is an unknown constant. Using Eqs. (21) and (2) into Eq. (16), the radial and hoop stresses are achieved as:

$$\sigma_r=C_1\left(B_1m_1r^{m_1-1}+B_2m_2r^{m_2-1}+B_3+3B_6r^2-\frac{B_5}{(1-m_1)(m_2-m_1)}\left(\ln(r)-\frac{1}{1-m_1}+1\right)+\frac{B_5}{(1-m_2)(m_2-m_1)}\left(\ln(r)-\frac{1}{1-m_2}+1\right)\right)+C_2\left(B_1r^{m_1}+B_2r^{m_2}+B_3r+B_6r^3+B_7A_2+B_8A_1-\frac{B_5r}{(1-m_1)(m_2-m_1)}\left(\ln(r)-\frac{1}{1-m_1}\right)+\frac{B_5r}{(1-m_2)(m_2-m_1)}\left(\ln(r)-\frac{1}{1-m_2}\right)\right)+C_3\frac{A_2}{r}+C_4\frac{A_1}{r}+\left(C_5-\lambda_1\right)\left(W_1\ln(r)+W_2\right)+\left(C_6-\zeta_1\right)\left(S_1\ln(r)+S_2\right) \tag{25}$$

$$\sigma_\theta=E_1\left(B_1m_1r^{m_1-1}+B_2m_2r^{m_2-1}+B_3+3B_6r^2-\frac{B_5}{(1-m_1)(m_2-m_1)}\left(\ln(r)-\frac{1}{1-m_1}+1\right)+\frac{B_5}{(1-m_2)(m_2-m_1)}\left(\ln(r)-\frac{1}{1-m_2}+1\right)\right)+E_2\left(B_1r^{m_1}+B_2r^{m_2}+B_3r+B_6r^3+B_7A_2+B_8A_1\right) \tag{26}$$

$$-\frac{B_5 r}{(1-m_1)(m_2-m_1)}\left(\ln(r)-\frac{1}{1-m_1}\right)+$$
$$\frac{B_5 r}{(1-m_2)(m_2-m_1)}\left(\ln(r)-\frac{1}{1-m_2}\right)$$
$$+E_3\frac{A_2}{r}+E_4\frac{A_1}{r}+\left(E_5-\lambda_1\right)\left(W_1\ln(r)+W_2\right)+$$
$$\left(E_6-\zeta_1\right)\left(S_1\ln(r)+S_2\right)$$

The unknown constants A_1, A_2, B_1, B_2, Z_1 and Z_2 can be determined by employing the magneto-electro-mechanical boundary conditions. The boundary conditions result in a system of six linear algebraic equations. These six algebraic equations are expressed in the form as:

$$X\begin{bmatrix}B_1 & B_2 & A_1 & A_2 & Z_1 & Z_2\end{bmatrix}^T=E, \tag{27}$$

where, the component of matrix X and E are presented in the Appendix A. Solving the system of equations results in obtaining the initial stresses, electric potential, magnetic potential and radial displacement analytically at zero time.

3.2 Creep analysis of MEE rotating disc

Considering the steady-state hygrothermal condition, differentiation Eq. (18) with respect to time yields:

$$\frac{\partial^2\dot{u}}{\partial r^2}+\frac{1}{r}M_1\frac{\partial\dot{u}}{\partial r}+\frac{1}{r^2}M_2\dot{u}=+M_7\frac{\dot{A}_2}{r^2}+M_8\frac{\dot{A}_1}{r^2}+$$
$$M_{14}r^{-1}\dot{\varepsilon}^c_{rr}+\frac{\partial\dot{\varepsilon}^c_{rr}}{\partial r}+M_{15}r^{-1}\dot{\varepsilon}^c_{\theta\theta}+M_{16}\frac{\partial\dot{\varepsilon}^c_{\theta\theta}}{\partial r} \tag{28}$$

Well-known Prandtl-Reuss equations relate the creep rates to the stresses as follows [27]:

$$\dot{\varepsilon}^c_r=\frac{\dot{\varepsilon}^c_e}{\sigma_e}\left(\sigma_r-0.5(\sigma_\theta+\sigma_z)\right)$$
$$\dot{\varepsilon}^c_\theta=\frac{\dot{\varepsilon}^c_e}{\sigma_e}\left(\sigma_\theta-0.5(\sigma_r+\sigma_z)\right) \tag{29}$$
$$\dot{\varepsilon}^c_z=\frac{\dot{\varepsilon}^c_e}{\sigma_e}\left(\sigma_z-0.5(\sigma_\theta+\sigma_r)\right)$$

where $\dot{\varepsilon}^c_i(i=r,\theta,\phi)$ is creep strain rate, $\dot{\varepsilon}^c_e$ is effective creep strain rate and σ_e is effective stress. Norton's law is considered as the creep constitutive model as [27]:

$$\dot{\varepsilon}^c_e=B(r)\sigma_e^{n(r)} \tag{30}$$

where material creep parameters *B(r)* and *n(r)* are function of radius as [27]:

$$B(r)=b_0 r^{b_1},\ n(r)=n_0 \tag{31}$$

where b_0, b_1 and n0 are constants. Regarding the plane stress condition and substituting Eq. (30) into Eq. (29) gives:

$$\dot{\varepsilon}^c_r=b_0 r^{b_1}\sigma_e^{n_0-1}\left(\sigma_r-0.5\sigma_\theta\right)$$
$$\dot{\varepsilon}^c_\theta=b_0 r^{b_1}\sigma_e^{n_0-1}\left(\sigma_\theta-0.5\sigma_r\right) \tag{32}$$
$$\dot{\varepsilon}^c_z=-(\dot{\varepsilon}^c_r+\dot{\varepsilon}^c_\theta)$$

The Von Mises equivalent stress is presented as:

$$\sigma_e=\sqrt{\sigma_r^2+\sigma_\theta^2-\sigma_r\sigma_\theta} \tag{33}$$

By the same way as in previous section, the solution of Eq. (28) can be considered as:

$$\dot{u}=D_1 r^{m_1}+D_2 r^{m_2}+G_1 r^{m_1}+G_2 r^{m_2}+B_7\dot{A}_2+B_8\dot{A}_1 \tag{34}$$

where $G_{1l}(r)$ and $G_{2l}(r)$ can be achieved using the method of variation of parameters as [21]:

$$G_{11}(r)=\frac{\sqrt{3}}{2}\frac{b_0}{m_2-m_1}\int\left\{\begin{matrix}r^{b_1-m_1}\sigma_e^{n_0}\left(\begin{matrix}M_{15}+\\M_{16}b_1-M_{14}-b_1\end{matrix}\right)+\\\left(M_{16}-1\right)r^{b_1-m_1+1}\dfrac{\partial\sigma_e^{n_0}}{\partial r}\end{matrix}\right\}dr$$
$$G_{21}(r)=-\frac{\sqrt{3}}{2}\frac{b_0}{m_2-m_1}\int\left\{\begin{matrix}r^{b_1-m_2}\sigma_e^{n_0}\left(\begin{matrix}M_{15}+\\M_{16}b_1-M_{14}-b_1\end{matrix}\right)+\\\left(M_{16}-1\right)r^{b_1-m_2+1}\dfrac{\partial\sigma_e^{n_0}}{\partial r}\end{matrix}\right\}dr \tag{35}$$

Now, rates of stresses, electric potential and magnetic potential can be gotten by differentiation Eqs. (14) and (16) with respect to time as:

$$\dot{\sigma}_r=C_1\frac{\partial\dot{u}}{\partial r}+C_2\frac{\dot{u}}{r}+C_3\frac{\dot{A}_2}{r}+$$
$$C_4\frac{\dot{A}_1}{r}-C_1\dot{\varepsilon}^c_{rr}-C_2\dot{\varepsilon}^c_{\theta\theta}, \tag{36-a}$$
$$\dot{\sigma}_\theta=E_1\frac{\partial\dot{u}}{\partial r}+E_2\frac{\dot{u}}{r}+E_3\frac{\dot{A}_2}{r}+$$
$$E_4\frac{\dot{A}_1}{r}-E_1\dot{\varepsilon}^c_{rr}-E_2\dot{\varepsilon}^c_{\theta\theta} \tag{36-b}$$
$$\frac{\partial\dot{\phi}}{\partial r}=L_1\frac{\partial\dot{u}}{\partial r}+L_2\frac{\dot{u}}{r}+L_3\frac{\dot{A}_2}{r}-$$
$$L_5\frac{\dot{A}_1}{r}-L_1\dot{\varepsilon}^c_{rr}-L_2\dot{\varepsilon}^c_{\theta\theta} \tag{36-c}$$
$$\frac{\partial\dot{\psi}}{\partial r}=P_1\frac{\partial\dot{u}}{\partial r}+P_2\frac{\dot{u}}{r}+P_3\frac{\dot{A}_1}{r}-$$
$$P_5\frac{\dot{A}_2}{r}-P_1\dot{\varepsilon}^c_{rr}-P_2\dot{\varepsilon}^c_{\theta\theta} \tag{36-d}$$

Substituting Eq. (34) into Eq. (36) and integrating Eqs. (36-c) and (36-d), after rearranging, gives:

$$\begin{aligned}\dot{\sigma}_r &= D_1\left(\left(m_1C_1+C_2\right)r^{m_1-1}\right)+D_2\left(\left(m_2C_1+C_2\right)r^{m_2-1}\right)+\\ &\left(C_2B_8+C_4\right)\frac{\dot{A}_1}{r}+\left(C_2B_7+C_3\right)\frac{\dot{A}_2}{r}+\\ &C_1\left(\frac{\partial G_{11}}{\partial r}r^{m_1}+G_{11}m_1r^{m_1-1}+\frac{\partial G_{21}}{\partial r}r^{m_2}+G_{21}m_2r^{m_2-1}\right)\\ &\quad+C_2r^{-1}\left(G_{11}r^{m_1}+G_{21}r^{m_2}\right)-\\ &b_0r^{b_1}\sigma_e^{n_0-1}\left(C_1\left(\sigma_r-0.5\sigma_\theta\right)+C_2\left(\sigma_\theta-0.5\sigma_r\right)\right)\end{aligned} \tag{37-a}$$

$$\begin{aligned}\dot{\sigma}_\theta &= D_1\left(\left(m_1E_1+E_2\right)r^{m_1-1}\right)+\\ &D_2\left(\left(m_2E_1+E_2\right)r^{m_2-1}\right)+\left(\left(E_2\right)B_8+E_4\right)\frac{\dot{A}_1}{r}\\ &+\left(\left(E_2\right)B_7+E_3\right)\frac{\dot{A}_2}{r}+\\ &E_1\left(\begin{array}{l}\frac{\partial G_{11}}{\partial r}r^{m_1}+G_{11}m_1r^{m_1-1}+\\ \frac{\partial G_{21}}{\partial r}r^{m_2}+G_{21}m_2r^{m_2-1}\end{array}\right)\\ &\quad+E_2r^{-1}\left(G_{11}r^{m_1}+G_{21}r^{m_2}\right)-\\ &b_0r^{b_1}\sigma_e^{n_0-1}\left(E_1\left(\sigma_r-0.5\sigma_\theta\right)+E_2\left(\sigma_\theta-0.5\sigma_r\right)\right)\end{aligned} \tag{37-b}$$

$$\begin{aligned}\dot{\phi} &= D_1r^{m_1}\left(L_1+\frac{L_2}{m_1}\right)+D_2r^{m_2}\left(L_1+\frac{L_2}{m_2}\right)-\\ &\left(B_8\left(L_2\right)-L_5\right)\ln(r)\dot{A}_1-\left(B_7\left(L_2\right)+L_3\right)\ln(r)\dot{A}_2\\ &+\int\left(\begin{array}{l}L_1\left(\begin{array}{l}\frac{\partial G_1}{\partial r}r^{m_1}+G_1m_1r^{m_1-1}+\\ \frac{\partial G_2}{\partial r}r^{m_2}+G_2m_2r^{m_2-1}\end{array}\right)+\\ L_2\left(+G_1r^{m_1-1}+G_2r^{m_2-1}\right)-\\ L_1\dot{\varepsilon}_{rr}^c-L_2\dot{\varepsilon}_{\theta\theta}^c\end{array}\right)dr+J_1\end{aligned} \tag{37-c}$$

$$\begin{aligned}\dot{\psi} &= D_1r^{m_1}\left(P_1+\frac{P_2}{m_1}\right)+D_2r^{m_2}\left(P_1+\frac{P_2}{m_2}\right)-\\ &\left(B_8\left(P_2\right)+P_3\right)\frac{r^{-\beta}}{\beta}\dot{A}_1-\left(B_7\left(P_2\right)-P_5\right)\ln(r)\dot{A}_2\\ &+\int\left(\begin{array}{l}P_1\left(\begin{array}{l}\frac{\partial G_1}{\partial r}r^{m_1}+G_1m_1r^{m_1-1}+\\ \frac{\partial G_2}{\partial r}r^{m_2}+G_2m_2r^{m_2-1}\end{array}\right)+\\ P_2\left(+G_1r^{m_1-1}+G_2r^{m_2-1}\right)-\\ P_1\dot{\varepsilon}_{rr}^c-P_2\dot{\varepsilon}_{\theta\theta}^c\end{array}\right)dr+J_2\end{aligned} \tag{37-d}$$

Using the boundary conditions, the unknown constants can be determined. The boundary condition of inner and outer radii of the MEE disc does not vary with the time, so there:

$$\begin{aligned}&\text{Fixed-Free}\rightarrow \dot{u}_r\big|_{r=a}=0,\quad \dot{\sigma}_r\big|_{r=b}=0,\\ &\text{Free-Free}\rightarrow \dot{\sigma}_r\big|_{r=a}=0,\quad \dot{\sigma}_r\big|_{r=b}=0,\\ &\dot{\phi}\big|_{r=a}=0,\quad \dot{\phi}\big|_{r=b}=0,\\ &\dot{\psi}\big|_{r=a}=0,\quad \dot{\psi}\big|_{r=b}=0.\end{aligned} \tag{38}$$

The resultant system of linear equations can be solved like as previous section. The details are presented in the Appendix A. To achieve history of stresses, electric and magnetic potential during creep progress, the rates of stresses, electric potential and magnetic potential are needed. First of all, a suitable time increment ($dt^{(i)}$) needs to be taken. The entire time is the sum of timing steps as the creep evolutions during the time. The total time after the i_{th} timing step can be presented as:

$$t_i=\sum_{k=0}^{i}dt^{(k)} \tag{39}$$

In the following time steps, the radial and hoop stress redistributions for former step are available, and then, the radial and hoop stress rates are acquired from Eqs. (37-a) and (37-b). Lastly, using an iterative method, the creep stress distribution can be achieved as:

$$\begin{aligned}\sigma_r^{(i)}(r,t_i)&=\sigma_r^{(i-1)}(r,t_{i-1})+\dot{\sigma}_r^{(i-1)}(r,t_{i-1})dt^{(i)}\\ \sigma_\theta^{(i)}(r,t_i)&=\sigma_\theta^{(i-1)}(r,t_{i-1})+\dot{\sigma}_\theta^{(i-1)}(r,t_{i-1})dt^{(i)}\end{aligned} \tag{40}$$

4. Numerical Results and Discussions

In this section, employing MATLAB software, the influence of various parameters on the creep response of MEE disc is investigated using some numerical examples. Material constants for the MEE can be found in Table 1 [5,27]. The inner radii a=0.04 m and outer radii b=0.15 m are taken for the disc. The following non-dimensional quantities are used for the numerical results:

$$\begin{aligned}&R=\frac{r-a}{b-a},\quad u^*=\frac{u(r)}{a},\quad \sigma_i^*=\frac{\sigma_i}{P_a},\ (i=r,\theta),\\ &\phi^*=\sqrt{\frac{\beta_{11}}{c_{11}}}\frac{\phi(r)}{b},\quad \psi^*=\sqrt{\frac{d_{11}}{c_{11}}}\frac{\psi(r)}{b}.\end{aligned} \tag{41}$$

Firstly, the creep evolution during the time is investigated. The boundary conditions are supposed as:

$$\begin{aligned}&\phi_a=0,\quad \phi_b=5000,\quad \psi_a=0,\quad \psi_b=0,\\ &T_a=0,\ T_b=50,\ M_a=0,\ M_b=0.5,\ \omega=30\pi\end{aligned} \tag{42}$$

Table 1. Material constants.

Property	Unit	Value
c_{11}	GPa	215
c_{12}	GPa	120
c_{23}	GPa	120
c_{22}	GPa	218
e_{11}	C/m^2	7.5
e_{12}	C/m^2	-2.5
α_r	1/K	6×10^{-6}
α_θ	1/K	15×10^{-6}
q_{11}	N/(Am)	345
q_{12}	N/(Am)	265
β_{11}	C^2/Nm^2	5.8×10^{-9}
d_{11}	Ns^2/C^2	95×10^{-6}
ε_{11}	Ns/VC	2.82×10^{-9}
β_r	m^3/kg	0.8×10^{-4}
β_θ	m^3/kg	1.2×10^{-4}
m_1	N/AmK	2.5×10^{-5}
χ_1	Cm/kg	0
P_1	C^2/m^2K	-2.5×10^{-5}
γ_1	Nm^2/Akg	0
n_0	-	3
b_1	-	-5
b_0	-	0.11×10^{-36}

Figs. 2 to 7 show the creep evolution of MEE disc under multiphysical loading for the Free-Free mechanical boundary condition. In this analysis, time increment $dt=5\times10^4$ s is used. It is observed that radial stress, electric potential and magnetic potential are constant during the time at the inner and outer radii of disc which satisfy the constant electro-magneto-mechanical boundary conditions. Concerning to Fig. 2, the tensile radial stress decreases with the time. Also, the location of maximum radial stress is changed during the time. Fig. 3 shows that the absolute value of circumferential stress is decreasing with time at the internal and external surface of the MEE disc during the time. Also, the location of maximum hoop stress is moved from internal surface toward middle of thickness. Fig. 4 illustrates that the effective stress is decreased with time significantly. Besides, the distribution of equivalent stress through the thickness becomes more uniform during the creep progress. Fig. 5 illustrates that the displacement rises with serving the time. According to Fig. 6, the maximum electric potential is decreased during the creep evolution. Since the disc is radially polarized, the radial stress redistribution has some effects on the electric potential distribution. Consequently, with the aim of condition monitoring, the electric potential histories may be used in the intelligent disc. Fig. 7 shows that the creep evolution has not

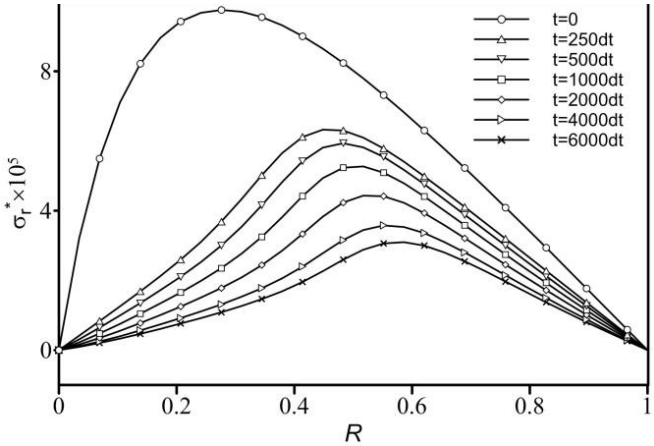

Fig. 2. Radial stress redistribution during creep progress (Free-Free)

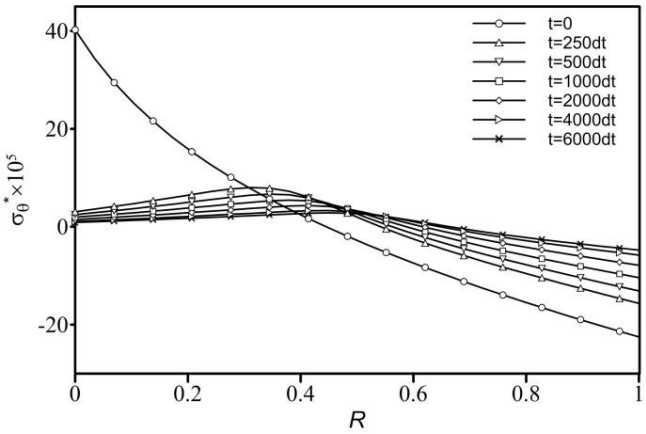

Fig. 3. Hoop stress redistribution during creep progress (Free-Free)

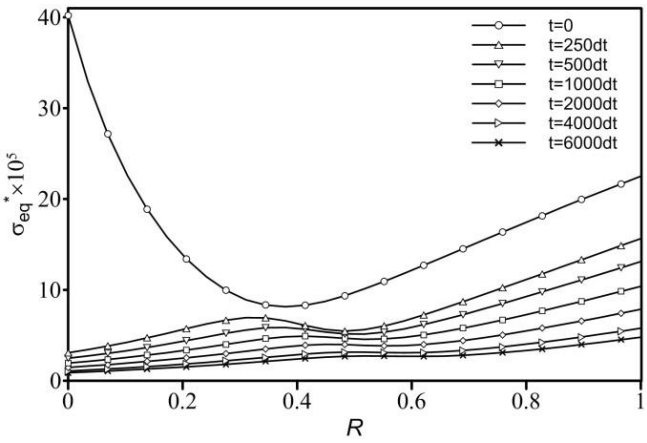

Fig. 4. Equivalent stress redistribution during creep progress (Free-Free)

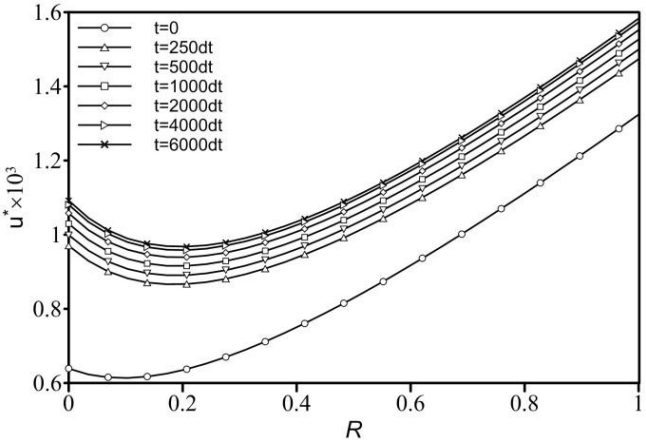

Fig. 5. Radial Displacement redistribution during creep progress (Free-Free)

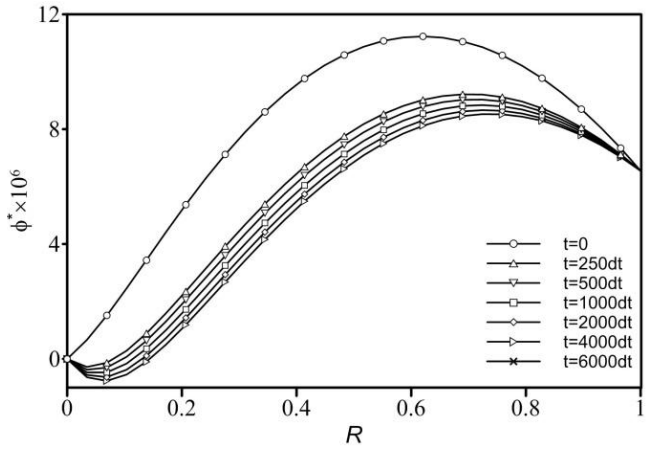

Fig. 6. Electric potential redistribution during creep progress (Free-Free)

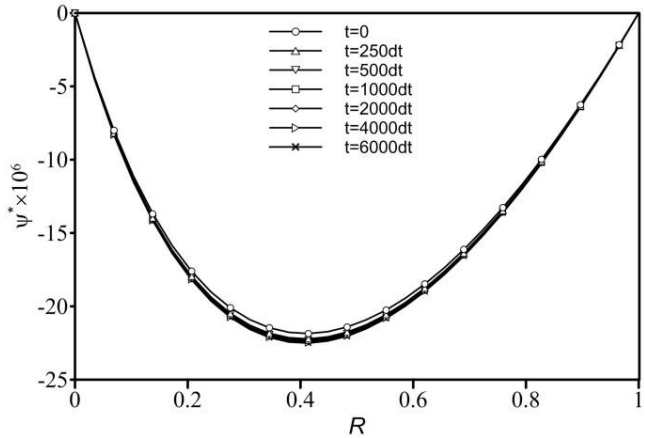

Fig. 7. Magnetic Potential redistribution during creep progress (Free-Free)

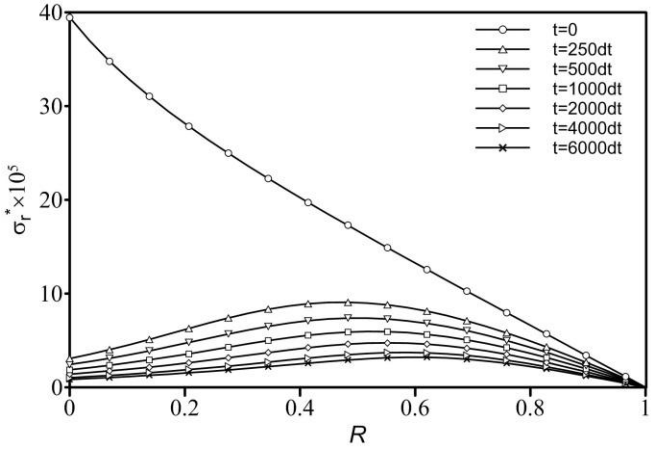

Fig. 8. Radial stress redistribution during creep progress (Fixed-Free)

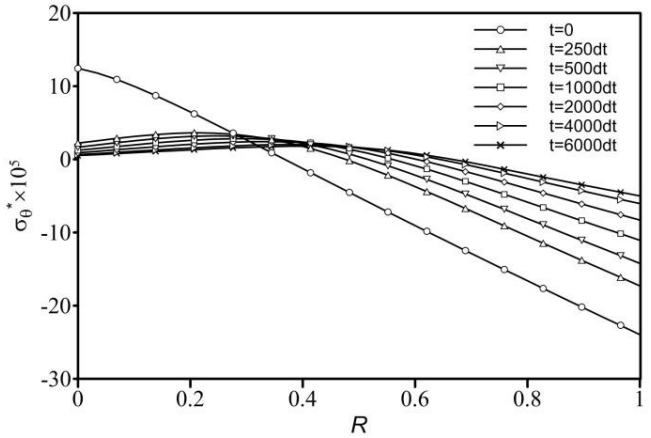

Fig. 9. Hoop stress redistribution during creep progress (Fixed-Free)

a significant effect on the distribution of magnetic potential.

Figs. 8 to 10 show the creep evolution of MEE disc for the Fixed-Free mechanical boundary condition. Other boundary conditions are as before case. It is observed that radial stress at the outer radii as well as the radial displacement at the inner radii is constant during the time which satisfies the Fixed-Free boundary conditions. Regarding Fig. 8, the tensile radial stress decreases with the time. Also, during the time, the location of maximum radial stress is changed from inner radii to middle of thickness approximately. Fig. 9 shows that the general behavior of hoop stress of the MEE disc during the time is similar to the previous case. Fig. 10 depicts that the radial displacement rises during the time. The enhancement is more considerable at outer radii.

The effect of temperature and humidity on the primitive and creep behavior of the MEE disc is disclosed in Figs. 11 to 15. The temperature and moisture concentration on the interior surface are taken as zero. However, the temperature and moisture concentration rise on the exterior surface (Mb=Tb/100). The Free-Free boundary condition is taken and other boundary conditions are same as before. According to Fig. 11, increasing in hygrothermal loading rises the tensile radial stress both for primitive and after creep evolution. Furthermore, changes in primitive radial stress are more

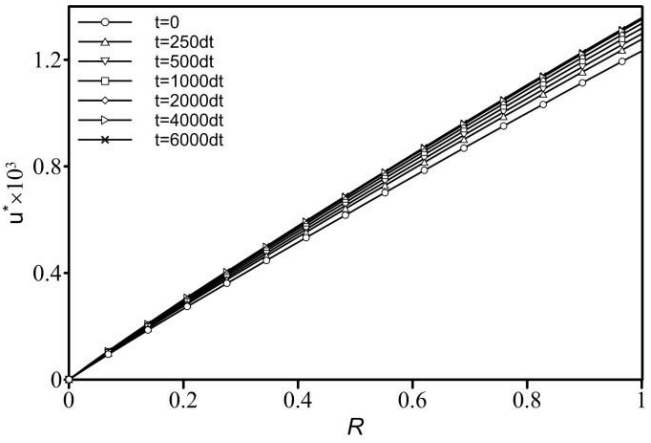

Fig. 10. Radial displacement redistribution during creep progress (Fixed-Free)

significant rather than creep one.

Fig. 12 depicts that, for primitive state, there is a fix point near the middle of thickness in which the circumferential stress does not change with change in hygrothermal loading. Before this point, rising in hygrothermal loading increases the tensile circumferential stress. While, after this point, it increases the compressive hoop stress. This enhancement must be considered in designing of MEE disc because high

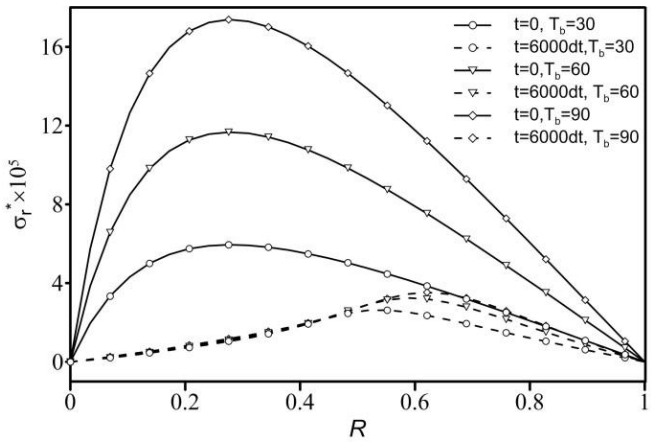

Fig. 11. Effect of hygrothermal loading on the initial and creep radial stress

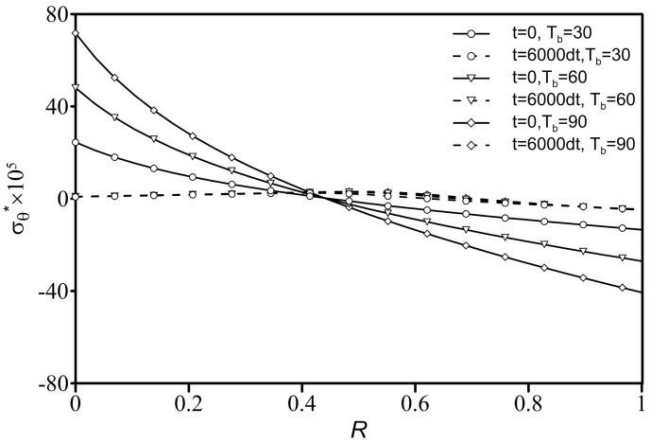

Fig. 12. Effect of hygrothermal loading on the initial and creep hoop stress

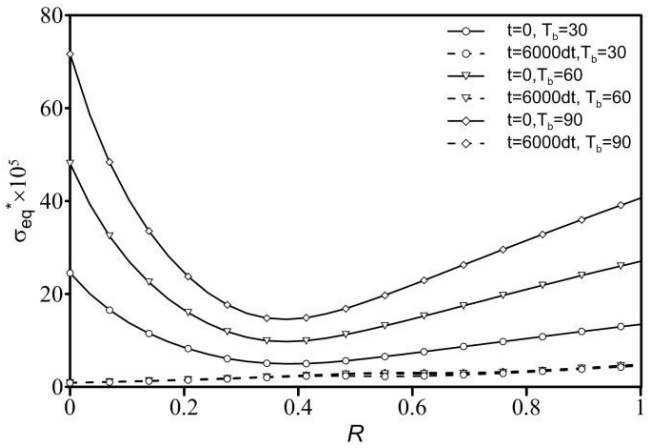

Fig. 13. Effect of hygrothermal loading on the initial and creep equivalent stress

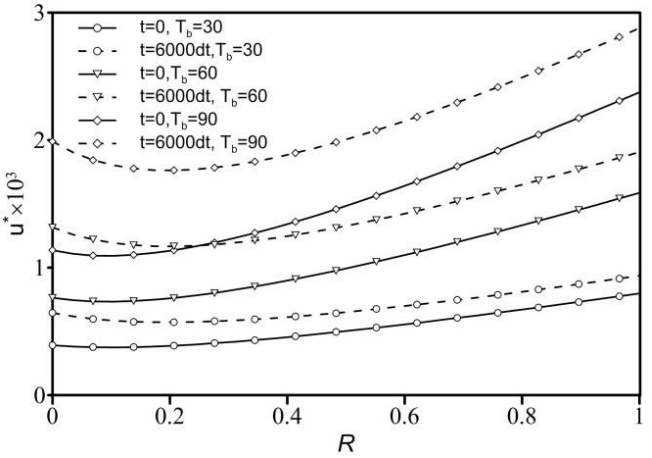

Fig. 14. Effect of hygrothermal loading on the initial and creep radial displacement

tensile hoop stress provides proper opportunity for cracking at the inner surface of MEE disc. The effect of hygrothermal loading on the hoop stress after creep evolution is insignificant according to Fig. 12. As observed in Fig. 13, for the primitive state, the effective stress is increased by increasing in hygrothermal loading. While, for the creep state, the effect of hygrothermal condition is inconsiderable. Fig. 14 reveals that an increase in applied hygrothermal loading results in an increase in both primitive and creep radial displacements. Fig. 15 demonstrated that rising in temperature and moisture concentration increases the maximum of electric potential for both initial and after creep evolution. The changes are more extensive in primitive case. In general, Figs. 11 to 15 implies that the effect of hygrothermal loading condition after creep evolution becomes less significant comparison with the static case.

For the next case, the influence of angular speed on the creep behavior is considered. The results are demonstrated in Figs. 16 to 19. Figs. 16 and 17 show that increasing in angular velocity has no considerable effect on the creep radial and hoop stresses. While, it increases the static radial and hoop stresses at increasing rate. According to Fig. 18, as the angular velocity rises, the initial effective stress increases at an increasing rate in the internal surface and decreases in the external surface. The angular velocity has no considerable effect on the effective creep stress. Fig. 19 depicts that increasing in angular velocity leads to an increase radial displacement in both initial and creep state. It can be concluded from Figs. 16 to 19 that generally the effect of angular velocity becomes less significant after creep progress.

To explore the influence of temperature- and moisture-dependent elastic coefficients on the response of MEE disc, the elastic coefficients can be expressed in the following form [25]:

$$C_{ij} = C_{ij\,0}(1+\alpha^* T + \beta^* M) \tag{43}$$

To avoid having non-linear equations, the temperature and moisture dependence is only assumed for the case that temperature and moisture concentration increase uniformly. So, the temperature and moisture concentration increases uniformly as: T=50, M=0.5. The Free-Free boundary condition is taken and other boundary conditions are kept unchanged. Figs. 20 to 23 reveals the influence of the hygrothermal dependence of the elastic coefficients on the initial and creep response of the MEE disc. Due to similarity of the effect of

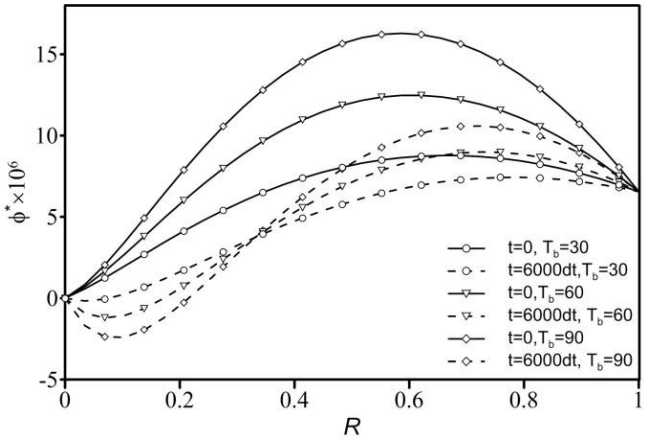

Fig. 15. Effect of hygrothermal loading on the initial and creep electric potential

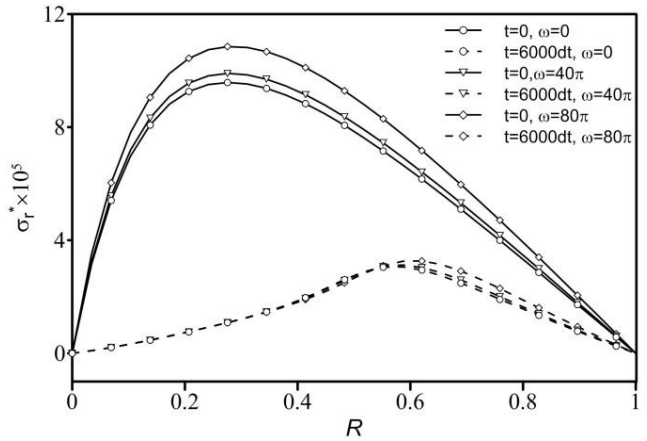

Fig. 16. Effect of speed of rotation on the initial and creep radial stress

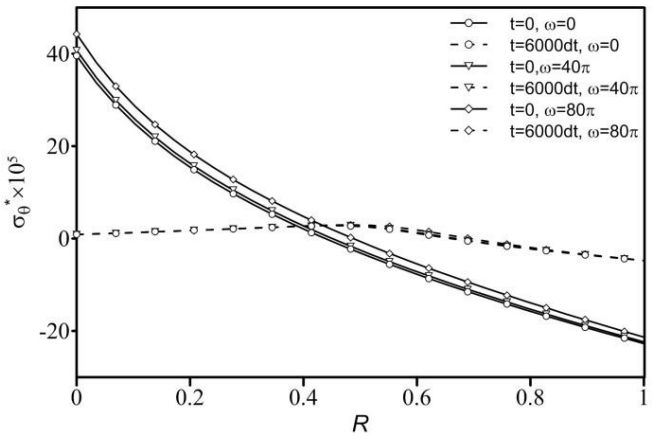

Fig. 17. Effect of speed of rotation on the initial and creep hoop stress

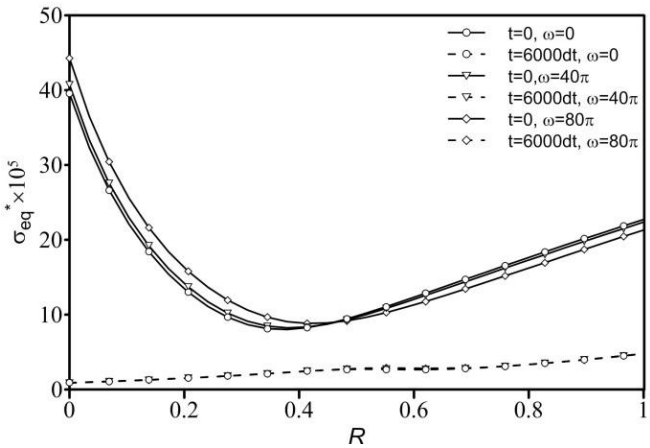

Fig. 18. Effect of speed of rotation on the initial and creep equivalent stress

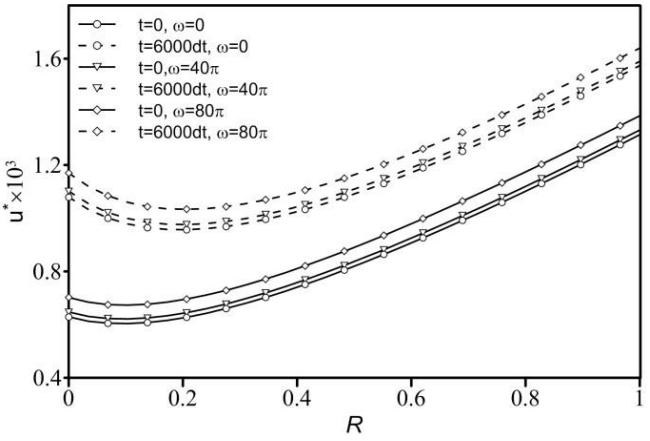

Fig. 19. Effect of speed of rotation on the initial and creep radial displacement

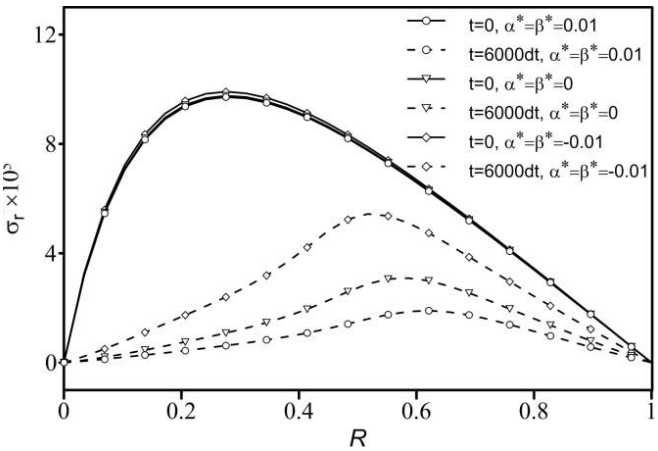

Fig. 20. Effect of hygrothermal dependency on the initial and creep radial stress

the temperature and humidity on the multiphysical behavior, the similar values are used for the empirical constants of temperature and moisture dependence. It is obvious that $\alpha^*=\beta^*=0$ indicates the material properties are independent of temperature and moisture. As shown in Figs. 20 to 23, the empirical constant has a negligible effect on the distribution of initial stresses and radial displacement of MEE disc. Fig. 20 shows that a positive empirical constant results in a reduction of creep radial stress. While, the effect of a minus value of empirical constant is vice versa. Fig. 21 depicts that the positive empirical constant reduces both the compressive creep hoop stress at the outer radii and tensile creep hoop stress at the inner radii. While, a negative empirical constant has an opposite influence. Fig. 22 shows the creep equivalent

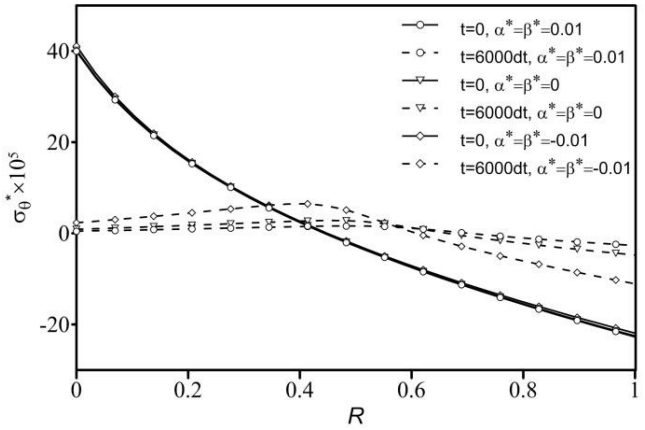

Fig. 21. Effect of hygrothermal dependency on the initial and creep hoop stress

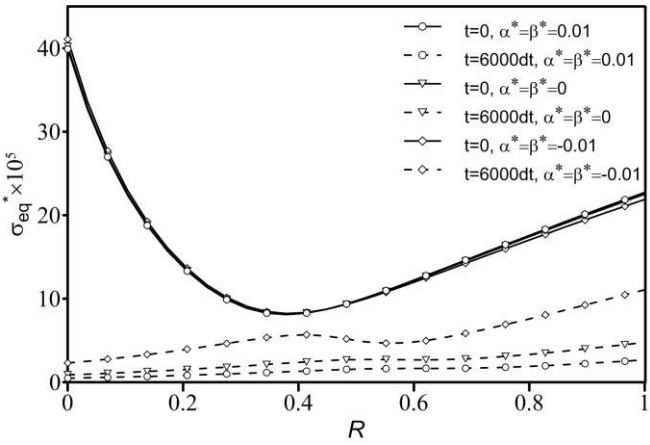

Fig. 22. Effect of hygrothermal dependency on the initial and creep equivalent stress

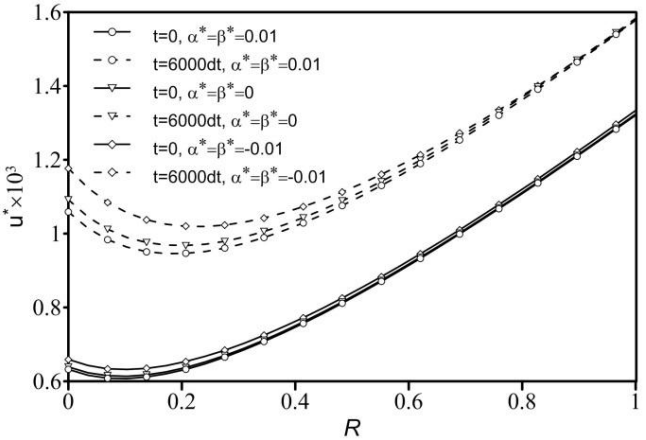

Fig. 23. Effect of hygrothermal dependency on the initial and creep radial displacement

stress rises (decreases) using negative (positive) value of empirical constant.

As observed in Fig. 23, using a positive empirical constant result in a reduction in radial displacement. While, using a negative one has a reverse effect. It can be concluded from Figs. 16 to 19 that analysis of the effect of temperature and moisture dependence after creep evolution is more important rather than initial state and it must be considered in the design progress.

5. Conclusion

In this article, a magneto-electro-elastic rotating disc subjected to an axisymmetric hygro-thermo-magneto-mechanical loading is considered. Applying the Prandtl-Reuss equations and Norton's law, the time-dependent creep behavior of the disk is analyzed analytically for the first time. The following conclusions can be expressed from the results:

1. The radial stress and absolute value of hoop stress decrease with the time in both Fixed-Free and Free-Free boundary conditions. While the radial displacement rises with serving the time.

2. Increasing in hygrothermal loading rises the initial radial stress, equivalent stress, radial displacement and maximum electric potential. Also, it increases the tensile hoop stress at the internal surface. Thus, to avoid cracking, this enhancement must be considered in design progress.

3. Increasing in angular velocity increases the initial radial and hoop stresses in addition to radial displacement at increasing rate.

4. Generally, the effect of hygrothermal loading and angular velocity becomes less significant after creep evolution comparison with static case.

5. Positive empirical constant of temperature- and moisture- dependency yields to a decrease in radial stress, absolute value of hoop stress, equivalent stress and radial displacement after creep evolution, while the negative value has an opposite effect.

6. The results imply that the effect of temperature- and moisture- dependence after creep evolution is more considerable and must be considered in the design progress.

Appendix A:

The component of matrix X and E for the primitive state with Free-Free boundary condition can be expressed as:

Also, for the Fixed-Free boundary condition, the following components are changed as:

Besides, for the state of creep progress, the components of X are as before case and the component of E for Free-Free boundary condition can be rewritten as:

Also, for the Fixed-Free boundary condition, the following components are changed as:

$$X_{11}=\left(C_1m_1+C_2\right)a^{m_1-1},\ X_{12}=\left(C_1m_2+C_2\right)a^{m_2-1},$$
$$X_{13}=\frac{C_4+C_2B_8}{a},\ X_{14}=\frac{C_3+C_2B_7}{a},$$
$$X_{15}=X_{16}=0$$

$$X_{21}=\left(C_1m_1+C_2\right)b^{m_1-1},X_{22}=\left(C_1m_2+C_2\right)b^{m_2-1},$$
$$X_{23}=\frac{C_2B_8+C_4}{b},X_{24}=\frac{C_2B_7+C_3}{b},$$
$$X_{25}=X_{26}=0$$

$$X_{31}=a^{m_1}\left(\frac{L_2}{m_1}+L_1\right),\ X_{32}=a^{m_2}\left(\frac{L_2}{m_2}+L_1\right),$$
$$X_{33}=\left(-L_5+L_2B_8\right)\ln(a),$$
$$X_{34}=\left(L_3+L_2B_7\right)\ln(a),X_{35}=1,\ X_{36}=0$$

$$X_{41}=b^{m_1}\left(\frac{L_2}{m_1}+L_1\right),\ X_{42}=b^{m_2}\left(\frac{L_2}{m_2}+L_1\right),$$
$$X_{43}=\left(-L_5+L_2B_8\right)\ln(b),$$
$$X_{44}=\left(L_3+L_2B_7\right)\ln(b),X_{45}=1,\ X_{46}=0$$

$$X_{51}=a^{m_1}(P_1+\frac{P_2}{m_1}),\ X_{52}=a^{m_2}(P_1+\frac{P_2}{m_2}),\tag{A1}$$
$$X_{53}=\left(-P_5+P_2B_8\right)\ln(a),$$
$$X_{54}=\left(P_3+P_2B_7\right)\ln(a),X_{55}=0,\ X_{56}=1$$

$$X_{61}=b^{m_1}(P_1+\frac{P_2}{m_1}),\ X_{62}=b^{m_2}(P_1+\frac{P_2}{m_2}),$$
$$X_{63}=\left(-P_5+P_2B_8\right)\ln(b),$$
$$X_{64}=\left(P_3+P_2B_7\right)\ln(b),X_{65}=0,\ X_{66}=1$$

$$E=\begin{bmatrix}-S_1(a)\\-S_1(b)\\\phi_a-S_2(a)\\\phi_b-S_2(b)\\\psi_a-S_3(a)\\\psi_b-S_3(b)\end{bmatrix}\tag{A2}$$

$$S_1=C_1\left(\begin{array}{l}B_3+3B_6r^2-\\\frac{B_5}{(1-m_1)(m_2-m_1)}\left(\ln(r)-\frac{1}{1-m_1}+1\right)\end{array}\right.$$
$$\left.+\frac{B_5}{(1-m_2)(m_2-m_1)}\left(\ln(r)-\frac{1}{1-m_2}+1\right)\right)+$$
$$C_2\left(B_3r+B_6r^3+B_7A_2+B_8A_1\right.$$
$$\left.\begin{array}{l}-\frac{B_5r}{(1-m_1)(m_2-m_1)}\left(\ln(r)-\frac{1}{1-m_1}\right)+\\\frac{B_5r}{(1-m_2)(m_2-m_1)}\left(\ln(r)-\frac{1}{1-m_2}\right)\end{array}\right)\tag{A3}$$
$$+\left(C_5-\lambda_1\right)\left(W_1\ln(r)+W_2\right)+$$
$$\left(C_6-\zeta_1\right)\left(S_1\ln(r)+S_2\right)$$

$$S_2=L_1\left(\begin{array}{l}B_3r+B_5+B_6r^3-\\\frac{B_5}{(1-m_1)(m_2-m_1)}\left(\mathrm{r}\ln(r)-2\mathrm{r}-\frac{r}{1-m_1}\right)\end{array}\right.$$
$$\left.-\frac{B_5}{(1-m_2)(m_2-m_1)}\left(r\ln(r)-2\mathrm{r}-\frac{r}{1-m_2}\right)\right)+$$
$$L_2\left(\begin{array}{ll}B_3r+\frac{B_6}{3}r^3 & -\frac{B_5r}{(1-m_1)(m_2-m_1)}\left(\ln(r)-1-\frac{1}{1-m_1}\right)+\\ & \frac{B_5r}{(1-m_2)(m_2-m_1)}\left(\ln(r)-1-\frac{1}{1-m_2}\right)\end{array}\right)\tag{A4}$$
$$+L_4\left(W_1r\ln(r)-W_1r+W_2r\right)+L_6\left(S_1r\ln(r)-S_1r+S_2r\right)$$

$$S_3=\psi(r)=P_1\left(\begin{array}{l}B_3r+B_5+B_6r^3-\\\frac{B_5}{(1-m_1)(m_2-m_1)}\left(\begin{array}{l}r\ln(r)-\\2\mathrm{r}-\frac{r}{1-m_1}\end{array}\right)\end{array}\right.$$
$$\left.-\frac{B_5}{(1-m_2)(m_2-m_1)}\left(r\ln(r)-2r-\frac{r}{1-m_2}\right)\right)+$$
$$P_2\left(\begin{array}{ll}B_3r+\frac{B_6}{3}r^3 & -\frac{B_5r}{(1-m_1)(m_2-m_1)}\left(\begin{array}{l}\ln(r)-\\1-\frac{1}{1-m_1}\end{array}\right)+\\ & \frac{B_5r}{(1-m_2)(m_2-m_1)}\left(\ln(r)-1-\frac{1}{1-m_2}\right)\end{array}\right)\tag{A5}$$
$$+P_4\left(W_1r\ln(r)-W_1r+W_2r\right)+P_6\left(S_1r\ln(r)-S_1r+S_2r\right)$$

$$X_{11}=a^{m_1},\ X_{12}=a^{m_2},\ X_{13}=B_8,$$
$$X_{14}=B_7,X_{15}=X_{16}=0$$

$$X_{21}=b^{m_1},X_{22}=b^{m_2},X_{23}=B_8,\tag{A6}$$
$$X_{24}=B_7,X_{25}=X_{26}=0$$

$$S_1=B_3r+B_6r^3-\frac{B_5r}{(1-m_1)(m_2-m_1)}\left(\ln(r)-\frac{1}{1-m_1}\right)+$$
$$\frac{B_5r}{(1-m_2)(m_2-m_1)}\left(\ln(r)-\frac{1}{1-m_2}\right)\tag{A7}$$

$$H\left[D_1\quad D_2\quad \dot{A}_1\quad \dot{A}_2\quad J_1\quad J_2\right]^T=E,\tag{A8}$$

$$E = -\begin{bmatrix} S_1(a) \\ S_1(b) \\ S_2(a) \\ S_2(b) \\ S_3(a) \\ S_3(b) \end{bmatrix} \tag{A9}$$

$$S_1 = C_1\left(\begin{matrix}\frac{\partial G_{11}}{\partial r}r^{m_1} + G_{11}m_1 r^{m_1-1} + \\ \frac{\partial G_{21}}{\partial r}r^{m_2} + G_{21}m_2 r^{m_2-1}\end{matrix}\right) + C_2 r^{-1}\left(G_{11}r^{m_1} + G_{21}r^{m_2}\right) - b_0 r^{b_1}\sigma_e^{n_0-1}\left(\begin{matrix}C_1\left(\sigma_r - 0.5\sigma_\theta\right) + \\ C_2\left(\sigma_\theta - 0.5\sigma_r\right)\end{matrix}\right) \tag{A10}$$

$$S_2 = \int\left(\begin{matrix}L_1\left(\begin{matrix}\frac{\partial G_1}{\partial r}r^{m_1} + G_1 m_1 r^{m_1-1} + \\ \frac{\partial G_2}{\partial r}r^{m_2} + G_2 m_2 r^{m_2-1}\end{matrix}\right) \\ + L_2\left(+G_1 r^{m_1-1} + G_2 r^{m_2-1}\right) - \\ L_1\dot{\varepsilon}_{rr}^c - L_2\dot{\varepsilon}_{\theta\theta}^c\end{matrix}\right)dr \tag{A11}$$

$$S_3 = +\int\left(\begin{matrix}P_1\left(\begin{matrix}\frac{\partial G_1}{\partial r}r^{m_1} + G_1 m_1 r^{m_1-1} + \\ \frac{\partial G_2}{\partial r}r^{m_2} + G_2 m_2 r^{m_2-1}\end{matrix}\right) \\ + P_2\left(+G_1 r^{m_1-1} + G_2 r^{m_2-1}\right) - \\ P_1\dot{\varepsilon}_{rr}^c - P_2\dot{\varepsilon}_{\theta\theta}^c\end{matrix}\right)dr \tag{A12}$$

$$S_1 = G_1 r^{m_1} + G_2 r^{m_2} \tag{A13}$$

Nomenclature

a	Inner radius of disc
b	Outer radius of disc
B_r	Magnetic induction [T]
C_{ij0}	Temperature and moisture independent elastic coefficient [N/m^2]
c_{ij}	Elastic coefficient [N/m^2]
D_r	Electric displacement [C/m^2]
d_{11}	Magnetic coefficient [N.s^2/C^2]
e_{1j}	Piezoelectric coefficient [C/m^2]
k^C	Moisture diffusivity coefficient
k^T	Thermal conductivity coefficient
m_1	Pyromagnetic coefficient [N/A.m.K]
p_1	Pyroelectric coefficient [C/m^2.K]
q_{1j}	Piezomagnetic coefficient [N/A.m]
χ_1	Hygroelectric coefficient [C.m/kg]

Greek symbols

α_i	Thermal expansion coefficient [1/K]
α^*	Empirical material coefficients for moisture dependence
β	Inhomogeneity parameter
β_i	Moisture expansion coefficient [m^3/kg]
β^*	Empirical material coefficients for temperature dependence
β_{11}	Dielectric coefficient [C^2/N.m^2]
γ_1	Hygromagnetic coefficient [N.m^2/A.kg]
ε_{11}	Electromagnetic coefficient [N.s/V.C]
λ	Thermal modulus [N/m^2.K]
ζ	Hygroscopic stress coefficient
ρ	Density [kg/m^3]
σ_i	Stress [N/m^2]
ϕ	Electric potential [W/A]
ψ	Magnetic potential [A]
ω	Rotating speed [rev/min]

References

[1] S. B. Singh, S. Ray, Modeling the anisotropy and creep in orthotropic aluminum-silicon carbide composite rotating disc, Mechanics of Materials, 34(6) (2002) 363-372.

[2] M. Saadatfar, Effect of Interlaminar Weak Bonding and Constant Magnetic Field on the Hygrothermal Stresses of a FG Hybrid Cylindrical Shell Using DQM, Journal of Stress Analysis, 3(1) (2018) 93-110.

[3] A. H. Akbarzadeh, Z. T. Chen, Hygrothermal stresses in one-dimensional functionally graded piezoelectric media in constant magnetic field, Composite Structure, 97 (2013) 317–331.

[4] M. N. M. Allam, A. M. Zenkour, R. Tantawy, Analysis of Functionally Graded Piezoelectric Cylinders in a Hygrothermal Environment, Advances in Applied Mathematics and Mechanics, 6(2) (2014) 233-246.

[5] M. Saadatfar, M. Aghaie-Khafri, Hygrothermomagnetoelectroelastic analysis of a functionally graded magnetoelectroelastic hollow sphere resting on an elastic foundation, Smart Materials and Structures, 23(3), (2014) 1-13.

[6] M. Saadatfar, M. Aghaie-Khafri, Electromagnetothermoelastic behavior of a rotating imperfect hybrid functionally graded hollow cylinder

resting on an elastic foundation, Smart Structures and Systems 15(6) (2015) 1411-1437.
[7] M. Saadatfar, M. Aghaie-Khafri, Hygrothermal analysis of a rotating smart exponentially graded cylindrical shell with imperfect bonding supported by an elastic foundation, Aerospace Science and Technology, 43 (2015) 37–50.
[8] M. Saadatfar, M. Aghaie-Khafri, On the magneto-thermo-elastic behavior of a FGM cylindrical shell with pyroelectric layers featuring interlaminar bonding imperfections rested in an elastic foundation, Journal of Solid Mechanics, 7(3), (2015) 344-363.
[9] M. Saadatfar, M. Aghaie-Khafri, Thermoelastic analysis of a rotating functionally graded cylindrical shell with functionally graded sensor and actuator layers on an elastic foundation placed in a constant magnetic field, Journal of Intelligent Materials Systems and Structures, 27 (2015) 512-527.
[10] M. Saadatfar, M. Aghaie-Khafri, On the behavior of a rotating functionally graded hybrid cylindrical shell with imperfect bonding subjected to hygrothermal condition, Journal of Thermal Stresses, 38 (2015) 854–881.
[11] M. Saadatfar, Effect of multiphysics conditions on the behavior of an exponentially graded smart cylindrical shell with imperfect bonding, Meccanica, 50 (2015) 2135–2152.
[12] A. M. Zenkour, Bending analysis of piezoelectric exponentially graded fiber-reinforced composite cylinders in hygrothermal environments, International Journal of Mechanics and Materials in Design, 13(4) (2017) 515–529.
[13] M. Vinyas, S. C. Kattimani, Hygrothermal Analysis of Magneto-Electro-Elastic Plate using 3D Finite Element Analysis, Composite Structures, 180 (2017) 617-637.
[14] T. Dai, H. L. Dai, Analysis of a rotating FGMEE circular disk with variable thickness under thermal environment, Applied Mathematical Modelling, 45 (2017) 900–924.
[15]V. K. Gupta, S.B. Singh, H.N. Chandrawat, S. Ray, Creep behavior of a rotating functionally graded composite disc operating under thermal gradient. Metallurgical and Materials Transactions A, 35 (2004) 1381–1391.
[16] D. Deepak, V. K. Gupta, A. K. Dham, Creep modeling in functionally graded rotating disc of variable thickness, Journal of Mechanical Science and Technology, 24(11) (2010) 2221-2232.
[17] M. Rattan, N. Chamoli and S.B. Singh, Creep analysis of an isotropic functionally graded rotating disc, International Journal of Contemporary Mathematical Sciences, 5(9) (2010) 419–431.
[18] D. Dharmpal, M. Garg, V.K. Gupta, Creep behavior of rotating FGM disc with linear and hyperbolic thickness profiles. Kragujevac Journal of Science, 37 (2015) 35–48.
[19] V. Gupta, S.B. Singh, Mathematical modeling of creep in a functionally graded rotating disc with varying thickness. Regenerative Engineering and Translational Medicine, 2(3) (2016) 126–140.
[20] T. Bose, M. Rattan, Effect of thermal gradation on steady state creep of functionally graded rotating disc, European Journal of Mechanics / A Solids, 67 (2018) 169–176.
[21] A. Loghman, M. Abdollahian, A. Jafarzadeh Jazi, A. Ghorbanpour Arani, Semi-analytical solution for electromagnetothermoelastic creep response of functionally graded piezoelectric rotating disk, International Journal of Thermal Sciences, 65 (2013) 254-266.
[22] A. Loghman and M. Azami, A novel analytical-numerical solution for nonlinear time-dependent electro-thermo-mechanical creep behavior of rotating disk made of piezoelectric polymer, Applied Mathematical Modelling, 40 (2016) 4795–4811.
[23] D. Zhou, M. Kamlah, Room-temperature creep of soft PZT under static electrical and compressive stress loading, Acta Materialia 54(5) (2006) 1389-1396.
[24] W. J. Chang, Transient hygrothermal responses in a solid cylinder by linear theory of coupled heat and moisture, Applied Mathematical Modelling, 18 (1994) 467-473.
[25] A.H. Akbarzadeh, Z.T. Chen, Magnetoelectroelastic behavior of rotating cylinders resting on an elastic foundation under hygrothermal loading, Smart Materials and Structures, 21 (2012) 125-133.
[26] M. Saadatfar, A.S. Razavi, Piezoelectric hollow cylinder with thermal gradient, Journal of Mechanical Science and Technology, 23 (2009) 45-53.
[27] H. L. Dai, H. J. Jiang, L. Yang, Time-dependent behaviors of a FGPM hollow sphere under the coupling of multi-fields, Solid State Sciences, 14 (2012) 587-597.
[28] S.A. Hosseini Kordkheili, R. Naghdabadi, Thermoelastic analysis of a functionally graded rotating disk, Composite Structures, 79 (2007) 508-516.